Charge and Energy Spectra of Trans-Iron Cosmic Rays

E. K. Shirk, P. B. Price,* and E. J. Kobetich†
Department of Physics, University of California, Berkeley, California 94720

W. Z. Osborne‡
Physics Department, Univ. of Houston, Houston, Texas 77004 and NASA Manned Spacecraft Center, Houston, Texas 77058

L. S. Pinsky, R. D. Eandi, and R. B. Rushing
NASA Manned Spacecraft Center, Houston, Texas 77058

(Received 26 October 1972)

A 22-m^2 detector array consisting of G-5 nuclear emulsion, fast-film Čerenkov detector, and 40 sheets of plastic detectors was exposed for $\sim$ 60 h at a mean atmospheric depth of $\sim$3.7 g/cm^2 and a rigidity of $<$2.5 GV. The detector was designed to determine both the charge and energy of trans-iron nuclei. For the first time it has been possible to determine cosmic-ray abundances in the difficult region $30 < Z \leq 42$ as well as to study the heavier nuclei. Over the entire periodic table from Ne on, the trend of cosmic-ray abundances is similar to that expected from sources with solar abundances, after nuclear reactions in interstellar space have been taken into account. The abundance ratios $[Z \geq 90]$:$[81 \leq Z \leq 83]$:$[74 \leq Z \leq 80]$ are not inconsistent with solar abundances if Grevesse's photospheric abundances of Th and U, adjusted for radioactive decay, are adopted instead of meteoritic abundances. These ratios agree somewhat better with an r-process composition and a leakage lifetime of several million years. No trans-uranic nuclei were observed in the present flight. Serious consideration must be given to the possibility that most of the cosmic rays with $Z < 60$ originate from material of solar composition. One of the major new results of the study was the determination of an energy spectrum for the nuclei with $Z > 60$. If the integral-energy spectrum is given by $N(>E) \propto (E + M_0c^2)^{-\eta}$, where E is the kinetic energy per nucleon, then the spectral index for high-Z nuclei is $\eta = 2.75 \pm 0.53$ for 0.5 GeV/amu $\leq E \leq$ 2.0 GeV/amu. In the same energy interval the index for helium nuclei is $\eta = 1.3$. This may imply a different origin for high- and low-Z cosmic rays.

I. INTRODUCTION

A series of balloon experiments in which nuclear emulsions and plastic track detectors were flown at high geomagnetic cutoff (4.6 GV) has revealed the charge spectrum of relativistic cosmic rays with $Z \gtrsim 50$ within the limitations of meager statistical accuracy.[1-8] The analyses depended on the earth's magnetic field to ensure that no primaries with $\beta \lesssim 0.9$ could reach the detector. The accuracy of charge measurement was limited by the uncertainty in velocity, and no information was obtained concerning the shape of the energy spectrum.

A flight from Sioux Falls with a very thick (10.5-g/cm^2) stack[5] established the velocity dependence of the etching rate in plastic, showed that the inherent resolution in plastic was excellent when β was known (from range measurement), and suggested that the spread between emulsion and plastic charge assignments in the Texas flights was mainly due to the uncertainty in velocity.

Calculations based on the results of the Sioux Falls flight indicated that in a plastic stack of $\sim$2 g/cm^2 thickness a heavy particle with energy $E \lesssim 1$ GeV/amu would slow sufficiently to allow determination of both energy and charge, provided its ionization rate were above threshold for the plastic detectors. The uncertainty in charge was expected to be nearly constant at $\Delta Z \simeq 2$. The uncertainty in energy would be very small for particles which stopped in the stack, but would increase with energy until at $E \gtrsim 1$ GeV/amu only a lower limit could be set. A typical value of ΔE for a particle with $Z = 70$ at 700 MeV/amu would be $\sim$50 MeV/amu.

Some time ago Badhwar, Deney, and Kaplon[9] conjectured that it might be possible to detect Čerenkov radiation from heavy nuclei with an extremely high-speed photographic emulsion. Detailed calculations and preliminary tests indicated that Eastman Kodak 2485 film has sufficient sensitivity to yield meaningful velocity information for $Z \gtrsim 60$. Consequently, fast-film Čerenkov detectors were designed and fabricated for the present experiment.

Our goals were to obtain new statistics for the charge distribution of cosmic rays with $Z > 50$, to study the unexplored region $30 < Z < 40$, and to determine for the first time an energy spectrum for high-Z cosmic rays. The inclusion of both a Lexan stack and a fast-film Čerenkov detector in some cases permitted independent determinations of velocities and provided a valuable test of both methods.

II. EXPERIMENTAL DETAILS

The detector stack shown in Fig. 1 consisted of one 200-μ Ilford G-5 emulsion, one fast-film Čerenkov detector, and 40 sheets of plastic. The plastic sheets were predominantly Lexan polycarbonate with a nominal thickness of 250 μ. A few sheets of 200-μ-thick unplasticized cellulose triacetate were also included. The total thickness was 1.7 g/cm^2 Lexan equivalent. The detector was arranged in eighty 30 cm×91 cm modules. Sixty-five of these modules, or a total effective area of 17.8 m^2, were studied in this experiment.

The detector array was launched from Minneapolis, Minnesota, on September 4, 1970. Owing to failures in all of the three separate descent mechanisms, the balloon became derelict after ~44 hours. After a 15-day, 5500-mile journey which extended to a point 1000 miles west of the Oregon coast, the balloon landed of its own accord near Regina, Saskatchewan, only about 600 miles from the launch point. Figure 2 shows the altitude and geomagnetic cutoff for the first 96 hours of flight. In our analysis we have assumed an exposure of 40 h at 2.8 g/cm^2 and 1.7 GV, followed by 20 h at 5.5 g/cm^2 and 2.1 GV. We neglected the subsequent exposure on the grounds that the depth in the atmosphere after 96 h was so great that nuclear interactions destroyed essentially all of the nuclei with $Z \gtrsim 48$.

A. Scanning Techniques

The region $26 < Z \lesssim 40$ has been difficult to study due to the large background of iron. The abundances fall five orders of magnitude across this region. None of the Texas flights produced reliable data for $Z \lesssim 50$. The counter telescopes of Webber[10] have recorded several events at $Z = 28$ and 30, but have not had sufficient collecting power to go beyond that point. The instrument of Binns *et al.*[11] does not resolve individual charges.

Unpublished measurements of stopping nuclei with $Z \approx 26$ to 30 indicated to us that plastic detectors can resolve charge peaks at the even-Z nuclei in this region. However, microscopic scanning techniques are far too slow to measure a sufficient number of ironlike events to ensure including among them some events with $Z \geq 29$. We have developed an extension of the ammonia-vapor technique[12] that discriminates against the iron background. This method permits us to locate a calculated fraction of events with $Z \gtrsim 28$ that come to rest in the stack. The energy interval sampled is ~300 to ~ 400 MeV/amu at the top of the atmosphere. Every fourth sheet in the main section of 30 sheets shown in Fig. 1 is etched for 160 h under controlled conditions. If the etching rate is sufficiently high, the cone tips meet and ammonia vapor passes through to form a spot on chemically sensitive paper over which the plastic sheet is taped. Events are selected by finding coincidences between adjacent pairs of fourth sheets. Since the etching rate is a rapidly decreasing function of velocity (and hence range), there exists a maximum range, $R_{max}(Z,A)$, for each element for which the tips meet for a standard etching time and sheet thickness. Furthermore, since the etching rate is a rapidly increasing function of charge, $R_{max}(Z,A)$ increases rapidly with charge. Figure 3 shows the values of $R_{max}(Z, A)$ for the etching time and sheet thickness used in this experiment. The result of a Monte Carlo calculation of the detection efficiency which allows for the angular distribution of the incoming particles and variations in the sheet thickness is also shown in Fig. 3. It has been assumed that the differential

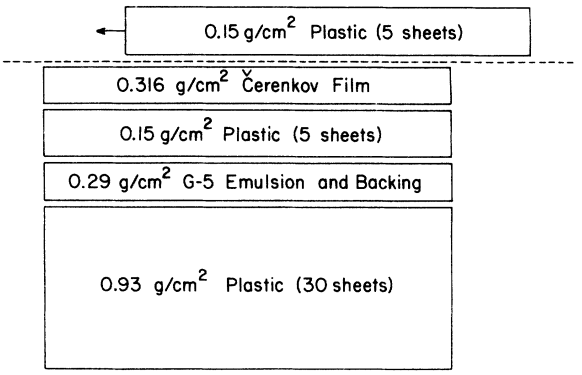

FIG. 1. Schematic drawing of the detector stack. The top five sheets were shifted when the balloon reached altitude.

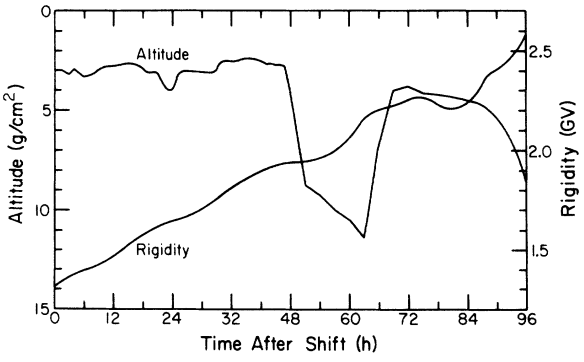

FIG. 2. Altitude and effective cutoff during the first 96 h of the flight. After 54 h, due to an instrument failure, the altitude had to be determined with a theodolite and is rather uncertain. After 96 h the atmospheric depth was greater than 10 g/cm^2.

energy spectra are nearly constant in the interval 300–400 MeV/amu.

The detection efficiency for Fe was independently determined for one of the modules by etching all of the sheets in that module and using the ammonia technique to locate all tracks that had etched through in 160 h. Events with $Z \geq 24$ and zenith angle less than 60° will produce detectable cylinders in at least one sheet near the end of their range. The relatively abundant nuclei – S, Si, and lighter elements – cannot produce cylinders in a 160-h etch even if at vertical incidence. Iron nuclei can thus be located with only a small admixture, mainly of Cr, Mn, and Ni. By this means we found that $\sim 5 \times 10^4$ Fe nuclei stopped in the volume of the detector in which every fourth sheet was scanned. Since only seven Fe tracks were detected by requiring coincidences between adjacent pairs of fourth sheets, the scanning efficiency becomes $(1.4 \pm 0.6) \times 10^{-4}$, which agrees well with the value calculated by the Monte Carlo method (Fig. 3).

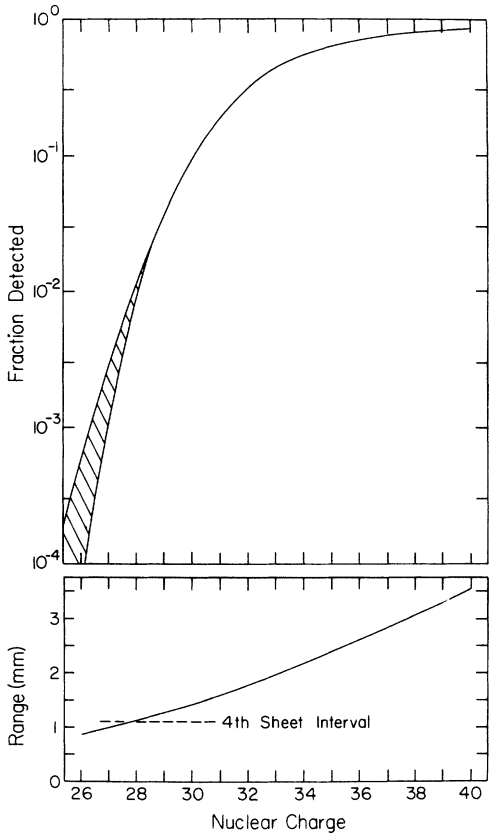

FIG. 3. Scanning efficiency for events with $26 \leq Z \leq 40$. In the lower section is shown the value of R_{max}, the maximum range at which a cylinder (connected cones) can occur for vertical events. The dashed line indicates the minimum range which can yield coincident cylinders when every fourth sheet is etched in an idealized stack with constant sheet thickness. Here all events with $Z < 28$ are rejected. The upper section of the figure shows the results of a realistic Monte Carlo calculation which allows for the angular distribution of incoming particles as well as for variations of sheet thickness. The measured efficiency for Fe was $(1.4 \pm 0.7) \times 10^{-4}$.

It should be emphasized that the detection efficiency with the ammonia scan of every fourth sheet is the result of a physical threshold in the detector and differs from the human efficiency for recognizing tracks of nuclei with $26 < Z \lesssim 40$ in nuclear emulsion.

The flux of nuclei with $42 \lesssim Z \lesssim 50$ is quite low; only one particle in this interval stopped in the 0.93-g/cm^2 stack thickness, and one stopped in the 0.15-g/cm^2 intermediate stack. Since the efficiency for visually locating these events in nuclear emulsion is likely to be less than 100%, we do not display the data in this interval in the final abundance graphs.

Both fast and stopping particles with $Z \gtrsim 42$ were found by visual scanning of the emulsion through low-power stereomicroscopes. The fourth-sheet ammonia technique was used as an independent method of finding very heavily ionizing events in the plastic.

B. Measurement of Charge with Lexan Detectors

Once the events were located, small sections of each sheet that included the particle's trajectory were cut out. A few sections were etched and measured in order to obtain preliminary estimates of charge and velocity. Then the remaining sections were etched for times selected so as to yield cones as long as possible without the tips meeting. In this way we avoided having to process the entire stack identically.

The etching was done in 40- and 200-liter tanks using 6.25N NaOH saturated with Lexan etch products.[13] A proportional controller was used to maintain the temperature at 40.00 ± 0.06 °C for periods of several hundred hours. The basic temperature reference was a calibrated high-grade mercury thermometer. Etching times were known to better than 0.1%.

Tracks were measured with a Leitz Ortholux microscope at 1600×. Vertical measurements were obtained with a Daytronic linear displacement transducer system coupled to a digital voltmeter and a printer. This system was frequently calibrated with a HeNe laser and a Fabry-Perot interferometer mounted directly on the microscope stage. Horizontal measurements were made with fine-lined reticles produced at the Lawrence Berkeley Laboratory.

The main measurement errors were in the judg-

ment of the operator as to the exact position of the cone tip. Computed values of the zenith angle of a track that passed through many sheets generally agreed to within 0.5°. The cone-length measurements made by several operators on a specific track generally agreed to within less than 1 μ.

The problem of determining the etching-rate response function $V_t(\beta,Z)$ for Lexan is made difficult by the lack of accelerators capable of producing beams of heavy particles at high energy. A successful approach,[5,14] for particles with energy greater than ~10 MeV/amu, has been to assume that the etching rate is a function of the ionization density

$$J(\beta, Z)=10^{-4}Z^{*2}\beta^{-2}[\ln(\beta^2\gamma^2)-\beta^2-\delta(\beta)+K], \quad (1)$$

where Z^* is the effective charge given by

$$Z^*=Z[1-\exp(-130\beta Z^{-2/3})], \quad (2)$$

and where $\delta(\beta)$ is an expression which takes into account the density effect for highly relativistic particles,[15] and K is an empirically determined constant. The etching rate along the track V_t has been found[5] to be related to J through a power law

$$V_t = BJ^{\gamma}, \quad (3)$$

where B and γ are empirical constants. Once the response function $V_t(\beta, Z)$ is established, the range-energy tables of Henke and Benton[16] can be used to calculate curves of $V_t(R,Z,A)$, where R is the range of the particle of charge Z and mass A corresponding to the velocity β.

Data used to determine B, γ, and K were obtained with 10.35-MeV/amu accelerator beams of Si, Ar, Ti, and Kr ions, as well as with cosmic-ray events in the iron peak. A comparison of these data with families of curves of V_t as a function of R for various values of K and γ shows that K must be so large as to completely dominate the other terms in the region of particle velocities involved. Thus the etching rate is given by the simple expression

$$V_t = B(Z^{*2}\beta^{-2})^{\gamma}. \quad (4)$$

The data in the cosmic-ray iron peak, which extend from ~20 to ~60 MeV/amu, were used to determine a best value of $\gamma = 2.05 \pm 0.14$ for the batch of Lexan used in the present experiment.[17]

The observable parameters of a track are the etched cone length L (which is corrected by adding the portion not visible because of bulk etching) and the residual range in the stack. It is convenient to work with the average track etching rate $\overline{V}_t = L/T$ and an average range $\overline{R}$ which is the range measured to the midpoint of the cone. The expression relating the etching rate to the cone length and the etching time T is

$$T = \int_{R_0}^{R_0+L} dR[V_t(R,Z,A)]^{-1}, \quad (5)$$

where R_0 is the range at the low-energy end of the cone. For $\gamma \approx 2$ the integral simplifies to the expression

$$T = L/V_t(R_0 + \tfrac{1}{2}L, Z, A). \quad (6)$$

The ranges of those particles which stop in the stack can be directly measured. A least-squares computer program is used to select that charge which gives the best agreement.

For particles which pass completely through the stack, the range at the bottom sheet R_b becomes an adjustable parameter. If the particle has an energy less than ~0.8 GeV/amu, the change in the etching rate over the thickness of the stack is large. A least-squares program varies both Z and R_b to find the best agreement.

The etching rate for very high-energy particles changes only slightly over the entire thickness of the stack. In this case the averages of the observed values of V_t and dV_t/dR are compared with calculated curves for different charges as a function of range, to determine the best values of Z and E. For energies above ~1 GeV/amu at the stack, it is possible only to place a lower limit on energy.

C. Measurements of Velocity with Fast-Film Čerenkov Detectors

The essential elements of the fast-film Čerenkov detector[18,19] include only a thin radiator and a sufficiently sensitive photographic film. A charged particle which traverses the radiator layer with a velocity greater than the phase velocity of light will emit Čerenkov radiation at an angle ψ with respect to its momentum. This Čerenkov angle is given by

$$\cos\psi = (n\beta)^{-1}, \quad (7)$$

where β is the particle velocity in units of c, and n is the index of refraction of the radiator. The intersection of the Čerenkov cone and the film plane yields an illuminated region which is a conic section with eccentricity

$$\epsilon = \sin\theta/\cos\psi, \quad (8)$$

where θ is the track zenith angle.

For this experiment each Čerenkov detector consisted of two opposed 12 in. × 12 in. sheets of Eastman Kodak 2485 film with a butylmethacrylate radiator layer between the sheets and in optical contact with both film emulsions. Each sheet of film contained an opaque (antihalation) coating between the emulsion and the Estar base. This served to

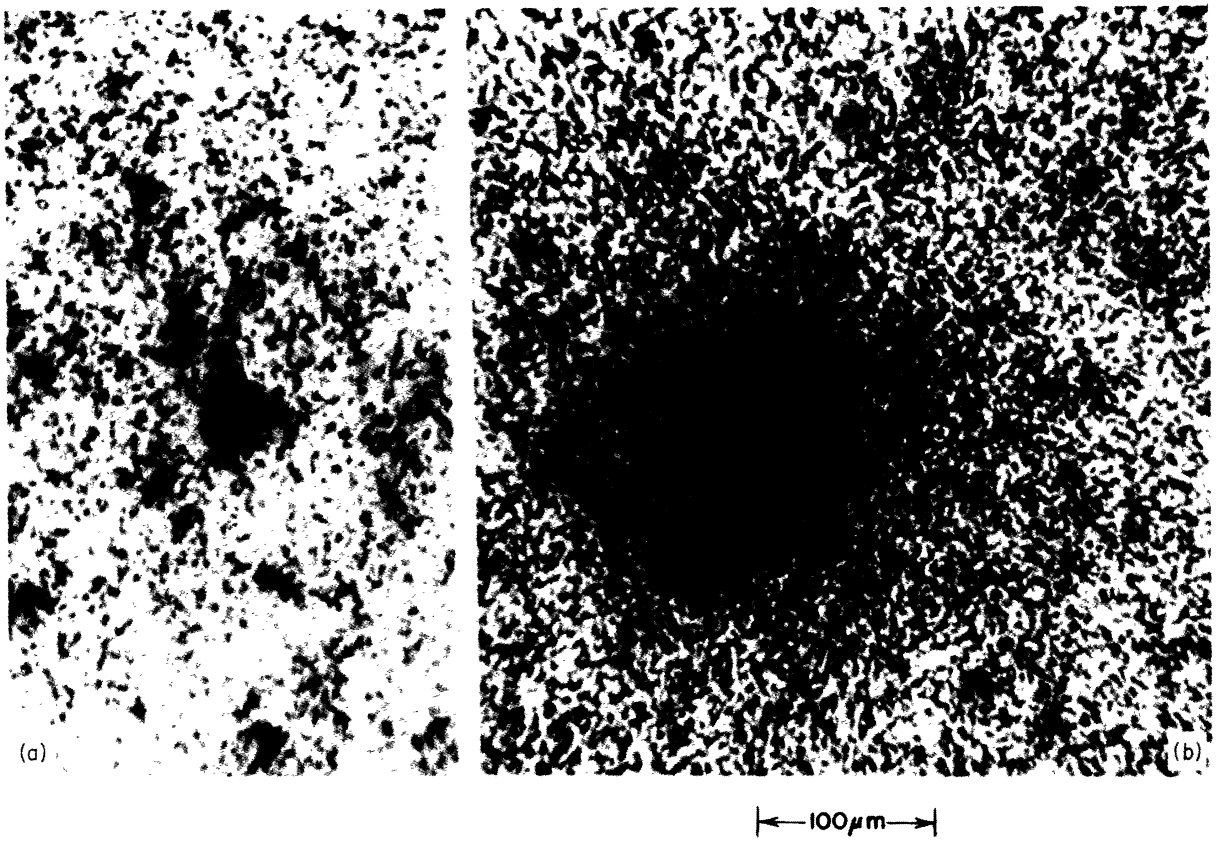

FIG. 4. (a) Photomicrograph of a typical Čerenkov image; (b) the corresponding upper-sheet ionization spot.

prevent any exposure of the emulsion from the base side.

For all zenith angles likely to be of interest, only the lower sheet of film receives Čerenkov light; thus, upper-sheet images must be due to ionization. We are persuaded that there is no contribution from scintillation in the radiator because all ionization spots seen in the upper sheets have diameters comparable to the core diameters of the corresponding nuclear emulsion tracks. Figure 4 contains photomicrographs of a typical Čerenkov image in a lower sheet and the ionization spot in the accompanying upper sheet.

The particle velocity can be derived from a known radiator thickness and a determination of the size of the Čerenkov conic section. Also, according to Eq. 8, the particle velocity can be obtained from a measurement of the eccentricity for nonzero zenith angles. In practice it is often impossible to resolve the entire Čerenkov image. In this case at least a portion of the boundary region of the observed image will be determined by a contour of constant exposure rather than by the edge of the Čerenkov conic section.

Each image was measured with a system known as AMID (Automated Microscope Image Dissector). Included in this system are an Image Dissector television camera, a microscope, and a Super Nova computer which controls both the camera and the microscope stage. A measurement yields a high-resolution (~5 μ) density map which is written on magnetic tape for input to a large computer. A χ^2 minimization program explored the full range of possible composite boundary regions to provide a best fit for each image map. The fit was obtained by varying the Čerenkov angle ψ and one other parameter, p/ρ. This second parameter is the number of Čerenkov photons generated per unit track length divided by the threshold sensitivity of the film. It is proportional to Z^2 and corresponds to the exposure contour that would determine the boundary region of the observed image for an infinitely thick radiator.

22 of the events with $Z > 50$ had corresponding fast-film Čerenkov detectors which survived intact and were usable. For the remaining events the Čerenkov detectors were either damaged during the balloon flight or during processing, or, as in the case of 12 events, the detectors have not yet been processed. Of the 22 events with usable

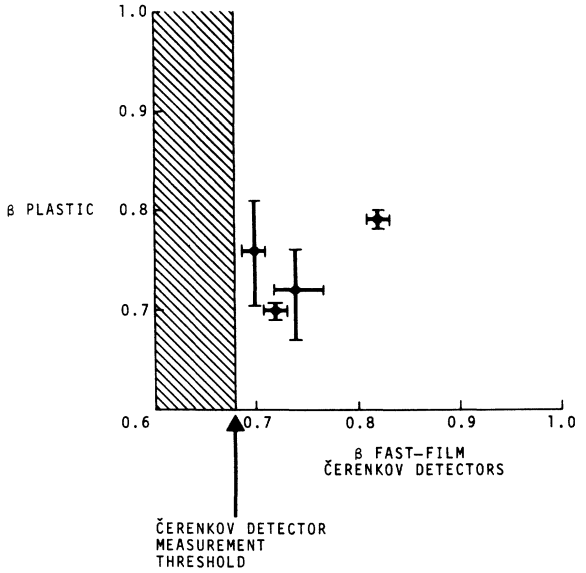

FIG. 5. Scatter plot of velocities measured in Lexan vs velocities from the fast-film Čerenkov detectors.

detectors, 5 resulted in Čerenkov images in the lower sheet. Each of the remaining 17 events generally produced only small (~5–10μ) ionization spots in both sheets. Either the particle velocity was below the Čerenkov threshold or its charge was too low ($Z<60$) to give sufficient Čerenkov light to leave a measurable image (the practical charge threshold of the Čerenkov detectors is Z~55–60).

Figure 5 compares the Čerenkov detector velocity assignments with the velocity assignments made from the ranges determined with the Lexan. One of the five events with Čerenkov images was found in the Čerenkov detectors and in the nuclear emulsion, but was not found in the Lexan. This event was not plotted in Fig. 5. In addition to exhibiting the generally satisfactory agreement between the two methods of velocity measurement, we note that no definitely fast ($\beta>0.7$) particles with $Z>60$ for which the corresponding fast-film Čerenkov detectors were usable have failed to yield Čerenkov images. A detailed examination of the actual images indicates that the usable velocity threshold of the Čerenkov detectors is $\beta\sim0.68$.

Figure 6 is a scatter plot of $(p/\rho)^{1/2}$ versus Z. Since $p/\rho\propto Z^2$, we expect a linear correlation. The results are consistent with this expectation and indicate a new method of charge estimation. However, calibration difficulties probably imply a noncompetitive charge resolution.

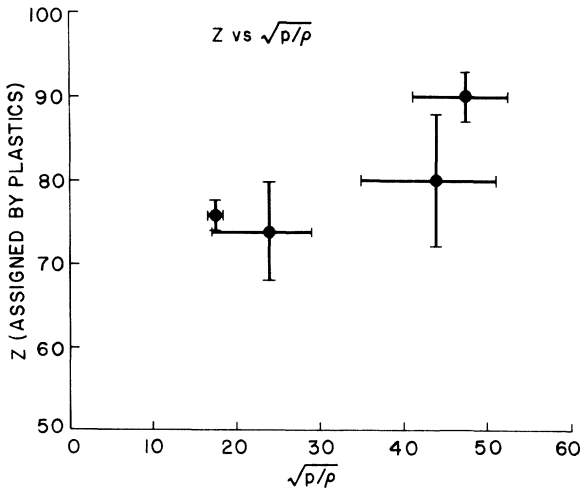

FIG. 6. Scatter plot of charges measured in Lexan vs corresponding values of $(p/\rho)^{1/2}$ from the fast-film Čerenkov detectors.

III. RESULTS

The histograms in Fig. 7 show the distribution of charges measured in Lexan for events found by visually scanning the nuclear emulsion. The histogram of "fast" events must be corrected for nuclei with Z, β, and zenith angle θ such that they pass through the Lexan without producing etchable tracks. From Eqs. (1)–(3) and the criterion that $V_t\cos\theta$ must exceed V_t (the bulk etching rate of Lexan) we have calculated the geometrical factor for track measurability in Lexan. Starting with an isotropic distribution at the top of the atmosphere,

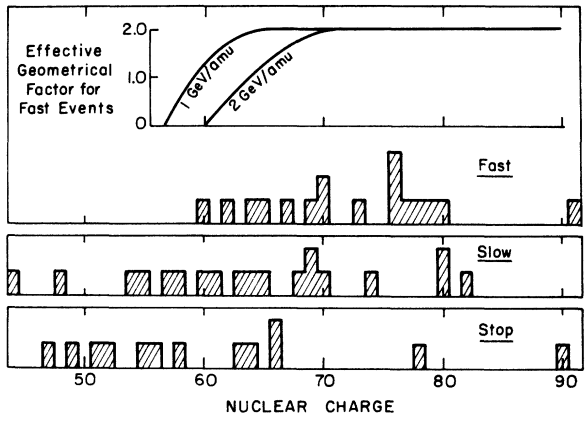

FIG. 7. Charges of particles with $Z>44$ measured in the plastic. The division between slow and fast particles is chosen at ~ 800 MeV/amu at detector altitude. The geometrical factor is a function of charge and velocity. The perpendicular component of the etching rate must exceed the bulk etching rate in order for the tracks to be revealed. The upper curve includes the effect of atmospheric breakup as well as the Lexan etching rate response at 1.0 GeV/amu and 2.0 GeV/amu.

we have taken into account the variation with zenith angle of the fraction of nuclei that survive to detector level. The geometrical factor at the detector is

$$F = \pi S\left[1-\left(\frac{64.5\beta}{Z}\right)^{8}\right], \tag{9}$$

where S is the collector area. The curve at the top of Fig. 7 takes into account both the geometrical factor and the effect of increased atmospheric breakup at large zenith angles.

The paucity of fast events with $Z \lesssim 65$ on the histogram is thus understood in terms of Lexan response and can be eliminated in the future when our facility for densitometric measurements on the tracks in the nuclear emulsion becomes operational.

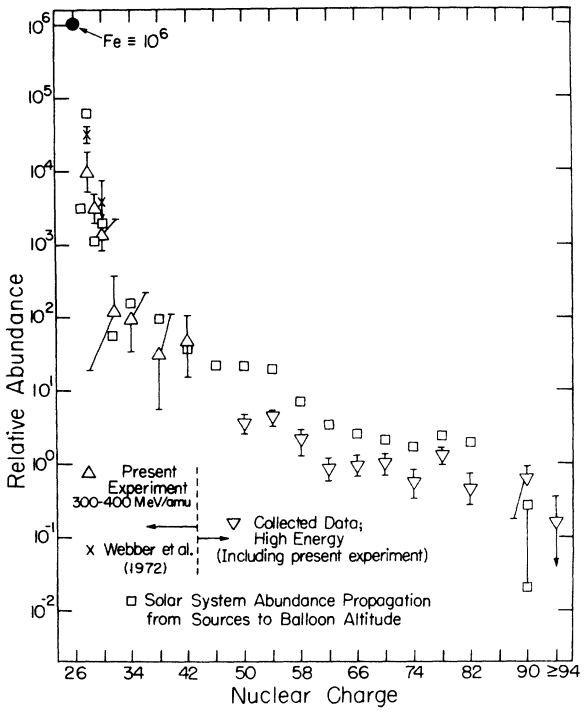

FIG. 8. Abundances of cosmic rays with $Z \geq 26$ at detector level (~ 3 g/cm^2). In the region $26 \leq Z \leq 42$, the triangles give fluxes of particles with 300–400 MeV/amu that stopped in the Lexan stack; the X at Ni was obtained by Webber *et al.* (Ref. 10), at energies greater than 250 MeV/amu. For $Z > 42$ the symbols ▽ give data compiled from flights at Palestine, Texas (Ref. 1,3,4,6–8) ($E \gtrsim 1.1$ GeV/amu), Sioux Falls, South Dakota (Ref. 5) ($E \gtrsim 500$ MeV/amu), and the present work. The squares are the result of propagating solar system abundances to the detector level through an exponential path-length distribution with a mean path length of 5 g/cm^2. In the region $26 \leq Z \leq 31$ the values are given at each charge; in the region $32 \leq Z \leq 84$ the value at each fourth charge includes a contribution from the previous two charges and the next higher charge. The value at $Z = 90$ includes Th and U; the higher point is based on a spectroscopic determination and the lower point is based on carbonaceous chondrite abundances.

Figure 8 displays abundance data for all trans-iron nuclei, normalized so that [Fe] = 10^6. In the region $28 \lesssim Z \lesssim 42$ are plotted our data for nuclei that had a kinetic energy of 300–400 MeV/amu at the top of the atmosphere and were found by ammonia-scanning every fourth sheet of Lexan. A point at $Z = 28$ obtained by Webber *et al.*[10] is included. For $Z > 42$, events have been found mainly by scanning emulsions, but in the region $42 \lesssim Z \lesssim 48$ no data are plotted because the efficiency for picking up events is almost certainly less than 100%. Above $Z \approx 48$, data from previous flights are regarded as adequate. Therefore, in the region $48 \lesssim Z < 62$, where we could not measure fast events in the Lexan, we have used previous data only. In the region $Z \geq 62$ all our data, together with previous data,[1,3–8] are included.

Figure 9 shows the integral energy spectrum for particles with $Z > 60$ compared with that of He nuclei at an equivalent level of solar activity. The measured zenith angle of the track, the average thickness of overlying material, and the range in the detector array were used to calculate the residual range of each detected particle at the top of the atmosphere. Appropriate range-energy relations[16] were applied to yield the corresponding energies. Though the statistics are less satisfactory, we have also computed the integral energy

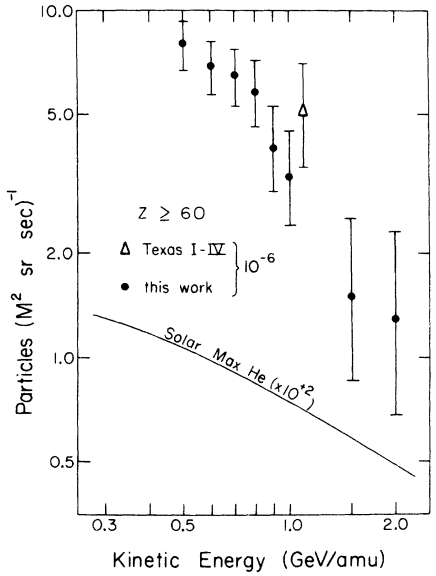

FIG. 9. Integral energy spectrum for particles with $Z > 60$. The spectrum falls much more steeply than the He spectrum at an equivalent level of solar activity.

spectrum for particles with $Z > 70$ and have found that it is similar in shape to that for particles with $Z > 60$ and much steeper than the He spectrum.

In calculating the flux, we corrected for nuclear interactions in the atmosphere and used the geometrical factor given by Eq. (9) to correct for tracks that could not be measured because the perpendicular component of V_t did not exceed V_g. At the low-energy end of the spectrum we also had to correct for the fact that only particles with a small zenith angle could penetrate to detector level and be identified.

Included in Fig. 9 is a point which represents the sum of the Texas flights. The energy was determined from the average geomagnetic cutoff of ~4.6 GV near Palestine, Texas. Since nuclei with $Z > 60$ retain their K electrons in interstellar space except at ultrarelativistic energies,[3] their mass/charge ratio when they approach the magnetosphere is $A/(Z-2) \approx 2.6$, which corresponds to a minimum energy at vertical incidence of 1.06 GeV/amu. Included for comparison is an integral energy spectrum of α particles measured at an equivalent level of solar activity. If the integral energy spectrum is given by $N(>E) \propto (E + M_0c^2)^{-\eta}$, where E is the kinetic energy per nucleon, then the spectral index for high-Z nuclei is $\eta = 2.75 \pm 0.53$ for 0.5 GeV/amu $\leq E \leq$ 2.0 GeV/amu. In the same energy interval the index for helium nuclei is $\eta = 1.3$.

IV. PROPAGATION

The charge spectra measured at balloon altitude do not directly represent the composition of the cosmic-ray sources. It is necessary to consider the effects of nuclear interactions, radioactive decay, and energy loss on the charge spectrum in the context of a reasonable propagation model.

We have used the steady-state diffusion model of Cowsik *et al.*[20] This results in a vacuum-path-length distribution which is a decreasing exponential,

$$P(x) = (1/x_0)\exp(-x/x_0). \tag{10}$$

Use of this simple model is justified in that it has yielded good fits[10] in the region $3 \leq Z \leq 26$ for values of x_0 between 4.0 g/cm^2 and 6.0 g/cm^2.

More complicated diffusion models which result in path-length distributions differing from the exponential have been proposed by Fichtel and Reames[21] and Ramaty and Lingenfelter.[22] The trans-iron nuclei are not useful in distinguishing between these models since they differ in their predictions primarily at large path lengths where both primary and secondary trans-iron nuclei have been destroyed in nuclear interactions in interstellar matter.

Indeed, the trans-iron nuclei are not useful even for determining the mean length x_0 of the exponential. In the nomenclature of Webber,[10] the effective slab length

$$x_{\text{eff}} = (\lambda^{-1} + x_0^{-1})^{-1} \tag{11}$$

is the harmonic sum of the vacuum mean path length x_0 and the interaction mean free path λ. Since λ is much smaller than x_0, the effective slab length x_{eff} does not depend on x_0 very strongly.

Models in which there are no very short path lengths, such as a Gaussian distribution centered at a finite path length or an exponential with a cutoff at 1.0 g/cm^2, lead to inconsistencies with our distribution of trans-iron nuclei. A path-length distribution that increases linearly to ~0.6 g/cm^2 and then declines exponentially has been proposed by Shapiro and Silberberg[23,24] to account for the secondaries lighter than Fe. This distribution also leads to strong inconsistencies when applied to the entire group of trans-iron nuclei and is definitely inferior to a pure exponential path-length distribution.

We have used two model source compositions. The first is the composition of the solar system, which is assumed to be representative of the composition of average interstellar material. For all of the elements up to Pb, we have followed the abundance table of Cameron,[25] which is based primarily on the chemical composition of primitive carbonaceous chondrites. The meteoritic abundance of Th is less than $\frac{1}{10}$ that recently determined in the solar photosphere by Grevesse.[26] Since calculations of heavy element abundances in the solar system by r-process nucleosynthesis agree much better with the spectroscopic value than with the meteoritic value, we have used the former as the preferred choice in our calculation. (We have also shown the meteoritic value as a second choice in Figs. 8 and 10.) From Grevesse's value of $[\text{Th}] = 0.21$ on the usual scale of $[\text{Si}] = 10^6$, we infer that $[^{232}\text{Th}] = 0.30$, $[^{235}\text{U}] = 0.30$, $[^{238}\text{U}] = 0.18$ for the solar-system abundances 4.6×10^9 yr ago, before radioactive decay. In the absence of a spectroscopic value for [U] in the sun, we used the relative production rates given by r-process theory.[27] A necessary consequence of high Th and U production is an increase in the r-process contribution to Pb and Bi, which results from the decay of short-lived elements with $Z \geq 84$. The value (before the decay of Th and U) is $[\text{Pb}]_r + [\text{Bi}]_r = 0.65$ on the scale of $[\text{Si}] = 10^6$. For the trans-uranic nuclides we assumed that all are in secular equilibrium between production at a steady rate by r-process synthesis in the galaxy and radioactive decay. The only nuclide with a

long enough half-life to warrant considering is ^{244}Pu, which in steady state would have an abundance of 0.002.

As a second model source composition we have used the r-process contribution to solar system abundances given by Seeger *et al.*,[27] thereby omitting any contribution from s-process synthesis. Such a source composition might be responsible for the cosmic rays with $Z \geq 36$, if they originate in highly evolved raw material. The values given by Seeger *et al.*[27] for [^{232}Th], [^{235}U], and [^{238}U] are 0.30, 0.26, and 0.18, respectively. For the trans-uranic nuclei we adopted an average of the values of Seeger *et al.* and of Schramm and Fowler,[28] normalized to [Th] + [U] = 0.78. The nuclides with the longest half-lives then have the abundances [^{237}Np] = 0.26, [^{244}Pu] = 0.12, and [^{247}Cm] = 0.08.

From the propagation of model source abundances, we have calculated predicted spectra at the detector. The results of these calculations were then compared with the experimental data. All stable isotopes were considered separately. Sums over charge groups were performed only at the end of the calculation. This method permits the most direct comparison with the data. In addition, information obtained about the expected distribution of masses at each charge is valuable in the experimental determination of charge for stopping particles, where the spread in mass limits the possible charge resolution.[5]

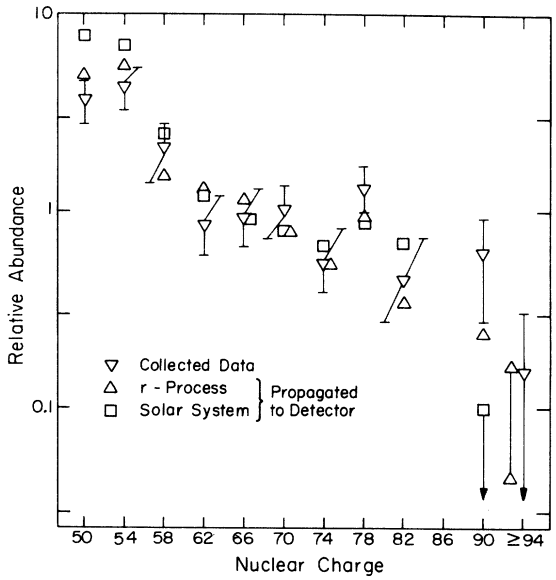

FIG. 10. The data are the same as in Fig. 8, but source distributions assumed to have solar system composition and r-process composition were propagated through an exponential path-length distribution and then normalized to the data in the region $60 \leq Z \leq 83$. The meteoritic abundance at $Z = 90$ is 0.020, too low to appear on the figure.

We assumed that the cosmic rays propagate in the galactic disk. The time scale which corresponds to a mean path length of ~5 g/cm^2 is then ~3×10^6 yr, assuming a mean matter density of ~1 atom/cm^3. All radioactive nuclei with mean lives $\ll 3 \times 10^6$ yr were assumed to decay, and all with mean lives $\gg 3 \times 10^6$ yr were treated in the same way as stable nuclei. The only nuclei with intermediate mean lives are ^{237}Np ($\tau = 3.1 \times 10^6$ yr) and ^{247}Cm ($\tau = 24 \times 10^6$ yr). Two values were used in Fig. 10 for the region $93 \leq Z \leq 96$. The higher value assumes that they do not decay, and the lower value that they do. (The initial abundances are low enough that secondaries may be neglected.) The equation describing the interaction network is

$$dN_i = -N_i \sigma_i^I N_o \, dx + \sum_{j \neq i} N_j \sigma_{ji} N_o \, dx, \tag{12}$$

where N_i is the density of particles of the ith stable nuclear species, σ_i^I is the total inelastic cross section, σ_{ji} is the cumulative partial cross section for the reaction $j \rightarrow i$ summed over short-lived intermediate nuclei, N_0 is Avogadro's number, and dx is the path length increment in g/cm^2.

We assumed that σ^I is given by the geometric cross section $\sigma^I \approx \sigma^G = 5 \times 10^{-26} A^{2/3}$ cm^2, where A is the mass number. The values for σ_{ji} were taken from Silberberg and Tsao.[29]

The cross sections are the major sources of uncertainty in the calculation. Silberberg and Tsao claim only about 50% accuracy for their semiempirical formulas, which in their original version tend on the average to overestimate the cross sections. This is evidenced by the consistent way in which the sum of σ_{ji} over products from $A_i = A_j - 1$ to $A_i \approx \frac{1}{2} A_j$ exceeds the geometric cross section. (In a recently modified version this tendency has been corrected.) The use of $\sigma^I \approx \sigma^G$ is an important source of error only if σ^I / σ^G is a function of the nuclear mass. The important quantities are σ_{ji}/σ_j^I and the ratio of the mean free path and the mean path length

$$\frac{\lambda}{x_0} = \frac{1}{N_0 \sigma^I x_0}. \tag{13}$$

If σ^I / σ^G is constant, then x_0 can be adjusted to produce results similar to those obtained with $\sigma^I / \sigma^G = 1$. The values of x_0 found for cosmic rays with $3 \leq Z \leq 30$ allow sufficient adjustment. However, a systematic variation of σ^I / σ^G with nuclear mass would produce a systematic shift in the calculated abundances.

The calculations do not include the effect of energy loss. The cross sections are evaluated at a

fixed high energy, $E = 2$ GeV/amu. The abundances are calculated numerically in 0.1-g/cm^2 increments out to a large value beyond which there is no effective contribution. These abundances are then summed over the assumed path-length distribution.

The atmospheric attenuation is accounted for by the factor $\exp[-\lambda_{air}/(4\,\mathrm{g/cm^2})]$, where λ_{air} is calculated with the geometric cross section, and 4 g/cm^2 is the atmospheric path length roughly averaged over zenith angles and atmospheric depths of various balloon flights. No assumptions are made concerning the partial cross sections in air since they are completely unknown. All atmospheric secondary production is neglected.

The results of the calculations normalized at iron are shown in Fig. 8 for the solar-system source abundances. In Fig. 10 the results with an r-process and a solar-system source are shown normalized to the collected data in the region $Z > 60$.

V. DISCUSSION

A. Velocity Determination with Fast-Film Čerenkov Detectors

Our results establish this method as a feasible means of determining the velocities of particles with $Z > 60$, $\beta > 0.68$. This makes it practical in high-Z cosmic-ray experiments to fly very thin detector stacks and to use the weight savings to fly larger areas at higher altitudes. The complexity in fabrication of the detectors discussed above and the corresponding high rate of damage during handling (both in balloon flying and processing) have led us to look for a more reliable design. Recently, Eastman Kodak succeeded in coating their 2485 photographic emulsion on a nonscintillating cellulose triacetate base (with no interface layers between the emulsions and the base). This film can be employed as a Čerenkov detector by using the film base as the Čerenkov radiator.

B. The Region $28 \leq Z \leq 42$

Previously only fragmentary information about the fluxes of nuclei just beyond Fe existed.[10,11] Though the statistics in the present experiment leave something to be desired, the abundance trends of these cosmic rays (at energies of 300–400 MeV/amu) and of trans-iron elements in the sun and meteorites appear to be quite similar (Fig. 8). Sources of cosmic rays must also follow a similar trend, because spallation of heavier nuclei into lighter nuclei can have had only negligible effects in this particular charge region where abundances increase with decreasing charge. With an exponential path-length distribution, ionization loss produces little relative distortion of abundances between sources and earth,[20] and we can safely neglect it. Unfortunately, little is known about the processes or sites of nucleosynthesis of the elements just beyond Fe, with the exception of Ni, which appears to be made simultaneously with Fe during Si burning.[30]

Now that there exists an effective Lexan scanning method to sieve out the nuclei with $28 \leq Z \leq 42$, additional statistics can be accumulated readily in future flights of thick, all-Lexan stacks at high altitude.

C. The Region $48 \leq Z \leq 92$

In this charge interval the sum of all balloon flight data are similar to solar system abundances propagated through an exponential path-length distribution, provided we use the spectroscopic Th value for the solar system (Fig. 8). Systematic discrepancies up to about a factor 2 should not be taken seriously, since an error this large could be attributed to uncertainties in the fluxes of Fe nuclei in various balloon flights. However, if a compelling case could be made for using the meteoritic U and Th values and rejecting the solar spectroscopic measurement[26] (which is supported by nucleosynthesis calculations), then the similarity would be seriously weakened. Of course, it might still be possible that the U and Th in our solar system are underabundant and atypical of the galactic gas, but the idea that cosmic rays might be a relativistic gas with average galactic composition would then lose some of its attractiveness.

By including low-energy data from the present flight with high-energy data, we have probably introduced a bias favoring the high-Z cosmic rays at the expense of Fe. In Fig. 9 we saw that the cosmic rays are richer in high-Z nuclei at low energy than at high energy relative to He. Though the integral Fe spectrum has not been as thoroughly studied as the integral He spectrum, the two appear to be similar in shape. As data on low-energy, high-Z cosmic rays accumulate in future flights, it will be necessary to quote separately the composition at low and at high energy so that the bias is more clearly seen. It will also be necessary to take ionization loss into account in the propagation.

By treating the level of heavy-element production relative to that of Fe and the lighter elements as a free parameter, we have attempted in Fig. 10 to improve the fit between source abundances and the data. In previous work it has been re-

TABLE I. Heavy-element abundances at detector level (taking [Si] ≈ [Fe] = 10^6).

Z	Observed	r-process origin (after 10^6 yr)	Gas of solar composition (4.6 Gyr ago)	Gas of meteoritic composition (4.6 Gyr ago)
72–79	1.3 ±0.2	1.9	4.2	4.2
80–83	0.3 ±0.1	0.42	1.9	1.9
90–92	0.4 ±0.1	0.28	0.27	0.022
≥93	0.15±0.1	0.17	0.003	3×10^{-4}

marked[3,6] that the relative abundances of the cosmic rays in the Pt group ($74 \leq Z \leq 80$), Pb group ($81 \leq Z \leq 83$), and U group ($90 \leq Z \leq 92$) resemble r-process ratios better than solar-system ratios. The difference is most noticeable for the U group in Fig. 10. Table I compares observed and predicted abundance ratios of those groups that are particularly useful for studying the lifetime and origin of cosmic rays.[3,31,32] Though the r-process ratios fit the data better, the solar-system ratios may perhaps be compatible with the data if the large uncertainties in absolute values of the assigned charges and the small number of events are considered.

D. Trans-Uranic Cosmic Rays

No trans-uranic cosmic rays were found in the present experiment, even though its collecting power was comparable to the total collecting power of all previous flights.

Four events have been reported previously. One of these[4] has been retracted as a result of further analysis.[7] A second one[6] passed through both emulsion and plastics, but the charge determined in emulsion ($Z \approx 104$) was quite different from the charge determined in plastic ($Z \approx 92$). The possibility that its true charge was 92 cannot be ruled out. A third one,[3] a fast nucleus that entered an emulsion stack launched at Palestine, Texas, was assigned a most probable charge $Z = 103$, with a very small probability that its velocity might have been low enough for its charge to be as low as 92. A fourth one[8] came to rest in a combined plastics-emulsion stack flown at Palestine, and its charge was estimated to be $Z \approx 96$.

Assuming that two of the events were trans-uranic, the flux of trans-uranic nuclei with $E \gtrsim 1$ GeV/amu is only ~0.01 $m^{-2}day^{-1}$. The entry in Table I for $Z \geq 94$ is thus an upper limit derived from this flux. One can see from Table I how important a definitive, measured flux of trans-uranic nuclei would be in deciding between a predominantly r-process composition and a predominantly solar composition. At the present time we must keep open the possibility that the charges of the two events in emulsion were overestimated and that definitive proof of the existence of trans-uranic cosmic rays is lacking.

E. Energy Spectrum of High-Z Cosmic Rays

Even before the present experiment, there was a hint of an enrichment of high-Z cosmic rays at low energies. In the Sioux Falls flight,[5] three out of four nuclei with $Z > 60$ were subrelativistic in energy. One of these three was a uranium nucleus.

The case for an excess of high-Z cosmic rays at low energy is much stronger in the present work. Nearly 20% of all events with $Z > 60$, including one of the two uranium nuclei, came to rest in the thin Lexan stack.

It is difficult to see how systematic errors in detecting the high-energy nuclei could account for the observed steep spectrum. About 1 m^2 of the emulsions was independently scanned by a second observer, who found no additional high-Z events. The ammonia-scan of every fourth sheet of Lexan turned up only one event (a nearly vertical, slowing nucleus with $Z \approx 56$) that had been missed in the emulsion scan.

At a given kinetic energy/amu, the rigidity of He is less than that of the high-Z nuclei, which have A/Z somewhat larger than 2. Thus, at low energies solar modulation flattens the He spectrum more than the high-Z spectrum, but this effect is far too small to contribute seriously to the observed difference between the two spectra.

An unknown portion of the flight occurred at atmospheric depths greater than 10 g/cm^2. If there were no nuclear interactions, ionization losses in the atmosphere would simply reduce the slope of the high-Z energy spectrum at detector level. Nuclear interactions would shift the charge distribution lower and build up the population of nuclei near the lower limit at $Z = 60$. Since this con-

tribution leads to a flattening of the high-Z spectrum, it cannot account for the striking difference in slopes of the curves in Fig. 9.

In view of the remarkable constancy of composition of the lighter nuclei He, CNO, LiBeB, and Fe as a function of energy, the steep spectrum of the high-Z nuclei is surprising and provides strong constraints on their origin, path-length distribution, and amount of ionization loss. With improved statistics from future flights, it will be important to establish how the spectrum steepens with increasing Z. Does it abruptly change immediately beyond the Fe peak or does it smoothly and continuously steepen all the way from Fe to the actinide region?

In recent solar-particle studies it has been found that heavy nuclei are enriched at low energies relative to their abundances at high energies. Conceivably there is a fundamental relationship between the two sets of data, although the enrichment of heavy-solar-particle abundances is observed to occur at much lower Z (~16 to 26) and at much lower energy ($\leq$ 10 MeV/amu) than for the heavy-cosmic-ray abundances.

F. Relevance to Models of Cosmic-Ray Origin

In this discussion we consider only two simple models at opposite extremes of a large variety of possible models. We first consider the possibility that the cosmic rays taken as a whole represent a homogenized sample of galactic composition, possibly distorted by selective emission and acceleration processes at the sources, followed by further distortion resulting from nuclear interactions during propagation. Though it now appears very unlikely that interstellar gas would be raised to relativistic energies through very inefficient Fermi acceleration processes, it has been suggested that interstellar gas at the periphery of white dwarfs[33] or pulsars might be efficiently accelerated by electromagnetic interactions with rotating magnetic fields.

The ratios [He]:[CNO]:[$Z>8$] are considerably different for cosmic rays and for solar-system material, but the relative abundances of all the elements beyond $Z \approx 8$ in cosmic-ray sources appear to be rather similar to abundances in meteorites and in the solar photosphere, and we have seen that this similarity appears to persist all the way to the end of the periodic table, with the possible exception of Th and U. Silberberg *et al.*[34] have independently pointed out this similarity. Recent studies[35] of solar-particle abundances at energies of ~10 MeV/amu show that they tend to differ from solar-photospheric abundances in much the same way as cosmic rays do. Though it is premature to discuss these differences in detail until long-term average trends of solar-particle abundances in many flares have been established, one is tempted to consider the possibility that a parallel exists between cosmic rays and galactic gas on the one hand and solar flare particles and the sun on the other hand.

At the other extreme of cosmic-ray models might be the long-standing view that both the abundances and the energy spectrum of cosmic rays are determined by explosive synthesis and acceleration during a supernova explosion. One naturally accounts for the depletion of the light elements H, He, C, N, and O, for the relative levels of the nuclei in the Pt, Pb, and U groups, and for the possible presence of trans-uranic cosmic rays in terms of nuclear reactions during the explosion. Unfortunately, it is extremely difficult to reproduce the observed abundances of the matter in our solar system even in a variety of thermonuclear processes, and so far no one has attempted the more difficult task of reproducing cosmic-ray abundances in a single process.

The high-Z nuclei play a crucial role in theories of the origin of cosmic rays. Better spectroscopic values for Th and U in the sun (including a redetermination of f values) would be extremely valuable in settling the present discrepancy between the solar and meteoritic abundances of Th and U. A definitive measurement of the relative abundance of trans-uranic cosmic rays would be even more important.

Instead of trying to arrive at a single explanation, it might be better to argue that a variety of sources are supplying cosmic rays, each effective in a limited region of energy and charge. Our observation of a steeper energy spectrum for the high-Z cosmic rays than for those from He up to Fe suggests that we may be dealing with at least two distinct types of cosmic-ray sources. The majority of primaries with $Z>60$ would originate in one of these and the lighter primaries would originate in the other. Price[36] has previously discussed the details of the high-Z distribution, and has pointed out that the positions and magnitudes of the peaks at $Z \approx 76$ and $Z \approx 54$ suggest r-process synthesis with a cycle time (<1 sec) much shorter than required to account for the abundances of elements in the solar system that are believed to be of r-process origin. In terms of our two extreme cosmic-ray models, we might associate the majority of the high-Z cosmic rays and their steep energy spectrum with the explosive phase of a supernova outburst, and the majority of the remaining cosmic rays with interstellar gas accelerated at the periphery of rotating magnetized objects.

ACKNOWLEDGMENTS

We are indebted to N. Peery and J. Steele for analyzing the tracks in plastics, to Robert Smith of Lawrence Berkeley Laboratory for processing the emulsions, to Otto Winzen and the staff of Winzen Research, Inc. for launching and recovering the balloon, to Professor P. H. Fowler and Professor W. A. Fowler for discussions, to Dr. R. Silberberg for his valuable comments on the manuscript, to Dr. D. E. Hagge for his support in initiating the experiment, and to the Atomic Energy Commission [Contract No. AT(04-3)-34] and to the National Aeronautics and Space Administration [Contracts Nos. NGR-05-003-376 and NGL-44-005-041] for financial support.

---

*Miller Institute Professor, 1972–73.

†Now at DuPont Experimental Station, Wilmington, Delaware.

‡NAS-NRC Senior Resident Research Associate at NASA/MSC when this experiment was initiated.

[1]P. H. Fowler, R. A. Adams, V. C. Cowen, and J. M. Kidd, Proc. R. Soc. Lond. A301, 36 (1967).

[2]G. E. Blanford, M. W. Friedlander, J. Klarmann, R. M. Walker, J. P. Wefel, W. C. Wells, R. L. Fleischer, G. E. Nichols, and P. B. Price, Phys. Rev. Lett. 23, 338 (1969).

[3]P. H. Fowler, J. M. Kidd, and R. T. Moses, Proc. R. Soc. Lond. A318, 1 (1970).

[4]G. E. Blanford, R. L. Fleischer, P. H. Fowler, M. W. Friedlander, J. Klarmann, J. M. Kidd, G. E. Nichols, P. B. Price, R. M. Walker, J. P. Wefel, and W. C. Wells, Acta Phys. Hung. 29, Suppl. 1, 423 (1970).

[5]D. O'Sullivan, P. B. Price, E. K. Shirk, P. H. Fowler, J. M. Kidd, E. J. Kobetich, and R. Thorne, Phys. Rev. Lett. 26, 463 (1971).

[6]P. B. Price, P. H. Fowler, J. M. Kidd, E. J. Kobetich, R. L. Fleischer, and G. E. Nichols, Phys. Rev. D 3, 815 (1971).

[7]G. E. Blanford, M. W. Friedlander, J. Klarmann, S. S. Pomeroy, R. M. Walker, J. P. Wefel, and W. C. Wells, in *Proceedings of the Twelfth International Conference on Cosmic Rays, Hobart, 1971* (Univ. of Tasmania Press, Hobart, Tasmania, 1971), Vol. 1, p. 269.

[8]P. H. Fowler, J. M. Kidd, E. K. Shirk, P. B. Price, and E. J. Kobetich, unpublished results.

[9]G. D. Badhwar, C. L. Deney, and M. F. Kaplon, private communication.

[10]W. R. Webber, S. V. Damle, and J. Kish, Astrophys. Space Sci. 15, 245 (1972).

[11]W. R. Binns, J. I. Fernandez, M. H. Israel, J. Klarmann, and R. A. Mewaldt, in *Proceedings of the Twelfth International Conference on Cosmic Rays, Hobart, 1971* (Univ. of Tasmania Press, Hobart, Tasmania, 1971), Vol. 1, p. 260.

[12]J. Blok, J. S. Humphrey, and G. E. Nichols, Rev. Sci. Instr. 40, 509 (1969).

[13]D. D. Peterson, Rev. Sci. Instr. 41, 1254 (1970).

[14]P. B. Price, R. L. Fleischer, D. D. Peterson, C. O'Ceallaigh, D. O'Sullivan, and A. Thompson, Phys. Rev. Lett. 21, 630 (1968).

[15]R. M. Sternheimer, Phys. Rev. 103, 511 (1956).

[16]R. P. Henke and E. V. Benton, U. S. Naval Radiological Defense Laboratory Report No. 1102, 1966 (unpublished).

[17]In a previous experiment (Ref. 5) the value $\gamma = 1.8 \pm 0.15$ was obtained. The difference may be due to the long, high-altitude exposure of the Minneapolis flight or to an intrinsic difference in the plastic which was manufactured at a different time.

[18]L. S. Pinsky, R. D. Eandi, W. Z. Osborne, and R. B. Rushing, in *Proceedings of the Twelfth International Conference on Cosmic Rays, Hobart, 1971* (Univ. of Tasmania Press, Hobart, Tasmania, 1971), Vol. 4, 1630.

[19]L. S. Pinsky, R. D. Eandi, R. B. Rushing, L. F. Thomson, and W. Z. Osborne, in Proceedings of the Eight International Conference on Nuclear Photography and Visual Solid-State Detectors, Bucharest, Rumania, 1972 (unpublished).

[20]R. Cowsik, Y. Pal, S. Tandon, and R. Verma, Phys. Rev. 158, 1238 (1967).

[21]C. E. Fichtel and D. V. Reames, Phys. Rev. 175, 1564 (1968).

[22]R. Ramaty and R. E. Lingenfelter, *Isotopic Composition of the Primary Cosmic Radiation*, edited by P. M. Dauber (Danish Space Research Institute, Lyngby, Denmark, 1971), p. 203.

[23]M. M. Shapiro and R. Silberberg, Ann. Rev. Astron. Astrophys. 8, 323 (1970).

[24]M. M. Shapiro, rapporteur's talk, in *Proceedings of the Twelfth International Conference on Cosmic Rays, Hobart, 1971* (Univ. of Tasmania Press, Hobart, Tasmania, 1971).

[25]A. G. W. Cameron, in *Origin and Distribution of the Elements*, edited by L. H. Ahrens (Pergamon, Oxford, 1968), p. 125.

[26]N. Grevesse, Sol. Phys. 6, 381 (1969).

[27]P. A. Seeger, W. A. Fowler, and D. D. Clayton, Astrophys. J. Suppl. 11, 121 (1965).

[28]D. N. Schramm and W. A. Fowler, Nature 231, 103 (1971).

[29]R. Silberberg and C. H. Tsao, Astrophys. J. Suppl. 25, 315 (1973).

[30]W. D. Arnett and D. D. Clayton, Nature 227, 780 (1970).

[31]D. N. Schramm, Astrophys. J. 177, 325 (1972).

[32]R. A. Mewaldt, R. E. Turner, M. W. Friedlander, and M. H. Israel, Acta Phys. Hung. 29, Suppl. 1, 423 (1970).

[33]R. Cowsik, in *Proceedings of the Twelfth International Conference on Cosmic Rays, Hobart, 1971* (Univ. of Tasmania, Hobart, Tasmania, 1971), Vol. 1, 329.

[34]M. M. Shapiro, R. Silberberg, and C. H. Tsao, Bull. Am. Phys. Soc. 17, 478 (1972).

[35]Summarized in a review paper by P. B. Price, in Proceedings of I. A. G. C. Cosmochemistry Symposium, Cambridge, Mass., 1972 (to be published).
[36]P. B. Price, rapporteur's talk, in *Proceedings of the Twelfth International Conference on Cosmic Rays, Hobart, 1971* (Univ. of Tasmania Press, Hobart, Tasmania, 1971).

PHYSICAL REVIEW D VOLUME 7, NUMBER 11 1 JUNE 1973

One- and Two-Particle Inclusive-Reaction Cross Sections in 13 GeV/c K^-p Collisions*

W. Barletta, M. Johnson, T. Ludlam, A. J. Slaughter, and H. D. Taft
Yale University, New Haven, Connecticut 06520
(Received 24 October 1972)

We present data for the production of $\pi^\pm$, K^0 (or $\overline{K}^0$), Λ, and Ξ^- particles in K^-p collisions at 13 GeV/c. We examine the behavior of the longitudinal and transverse components of single-particle momentum spectra, and the two-particle correlations, as functions of the masses and quantum numbers of the observed particles. The effects of resonance production and decay on the behavior of these distributions are studied.

I. INTRODUCTION

Ideas and predictions concerning limiting behavior of particle spectra in very-high-energy collisions[1] have generated considerable effort over the past few years in the study of inclusive processes of the type

$$a+b\to c+\text{anything}\,, \tag{1}$$

in which a single particle c is observed, summing over all final states. It has by now been amply demonstrated that, for the case in which particle c is a pion, the observed spectra (when displayed in the appropriate variables) become nearly independent of energy at very high energy.[2,4] For some reactions this limiting behavior is apparently manifested even for incident laboratory energies in the "intermediate" range of 10–30 GeV, provided the observed pion momentum falls in a kinematic region which may be associated with fragmentation of particle a or particle b.[3,4] It is to be expected that for secondary particles other than the pion this scaling behavior, particularly at intermediate energies, will depend strongly on the mass and quantum numbers of the observed particle, as well as the quantum numbers of the incident channel.

The promulgation of detailed models for multiparticle production[5] invites comparison between theory and experiment not only for the energy dependence of inclusive cross sections, but also for the shapes of distributions in all the kinematic variables for reaction (1), as well as for the more complex two-particle inclusive process

$$a+b\to c+d+\text{anything}\,. \tag{2}$$

As such models are developed it is clearly desirable to examine the general features of reactions (1) and (2) with as wide a variety as possible in the masses and quantum numbers of the incident and observed particles.

We present here the results of a study of single- and two-particle inclusive reactions in K^-p collisions at 12.6 GeV/c. The following reactions have been investigated:

$$K^-p\to \pi^\pm+\text{anything}, \tag{3}$$
$$\to K_n+\text{anything}, \tag{4}$$
$$\to \Lambda+\text{anything}, \tag{5}$$
$$\to \Xi^-+\text{anything}, \tag{6}$$
$$\to K_n+\pi^-+\text{anything}, \tag{7}$$
$$\to \Lambda+\pi^\pm+\text{anything}, \tag{8}$$
$$\to \Lambda+K_n+\text{anything}\,. \tag{9}$$

Here K_n refers to K^0 or $\overline{K}^0$ observed via the decay $K^0_S\to\pi^+\pi^-$. The data are from an exposure of the BNL 80-in. bubble chamber to a beam of rf-separated kaons, with a path length corresponding roughly to 6 events per microbarn of cross section within a restricted fiducial volume. All interactions recorded on film were measured, using the Yale PEPR system. Cross sections for the reactions listed above are given in Table I.[6] Here, and throughout this paper, the quoted error includes systematic as well as statistical uncertainties.

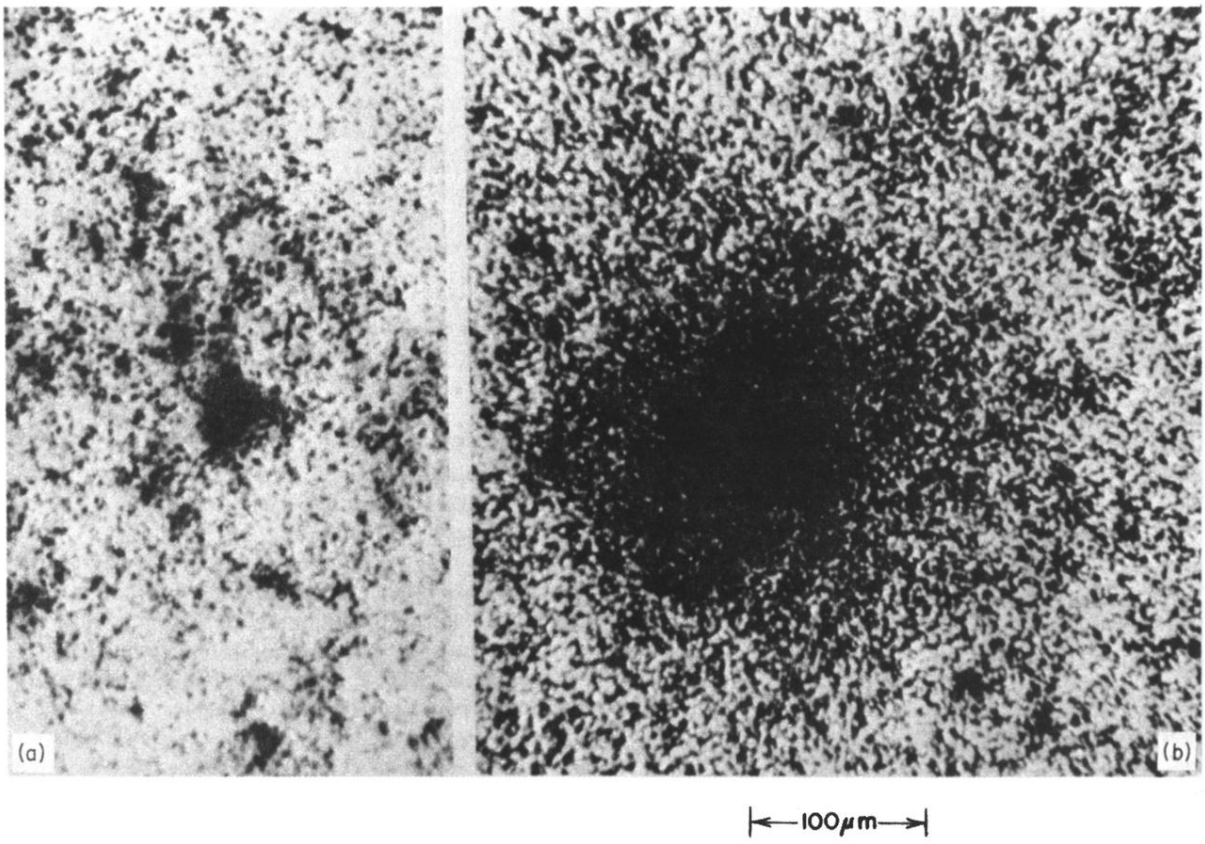

FIG. 4. (a) Photomicrograph of a typical Čerenkov image; (b) the corresponding upper-sheet ionization spot.